Geomorphology, 5 (1992) 39–57
Elsevier Science Publishers B.V., Amsterdam

Fluvial landsculpting and the fractal dimension of topography

Clement G. Chase
Department of Geosciences, University of Arizona, Tucson, AZ 85721, USA

(Received May 9, 1991; accepted after revision November 14, 1991)

ABSTRACT

Chase, C.G., 1992. Fluvial landsculpting and the fractal dimension of topography. In: R.S. Snow and L. Mayer (Editors), Fractals in Geomorphology. *Geomorphology*, 5: 39–57.

Quantitative models of landform development can help us to understand the evolution of mountains and regional topography, and the effects of tectonic motions and climate on landscape, including its fractal geometry. This paper presents a general and powerful three-dimensional model of fluvial erosion and deposition at hill- to mountain-range scale. The model works by accumulating the effects of randomly seeded storms or floods (precipitons) that cause diffusional smoothing then move downslope on digital topography grids, that erode portions of elevation differences, that transport a slope-limited amount of eroded material, and that deposit alluvium when their sediment-carrying capacity is exceeded.The iteration of these simple and almost linear rules produce very complicated simulated landscapes, demonstrating that complex landscapes do not *require* complex laws. Each process implemented in the model is affected differently by changes in horizontal scale. Erosion, a scale-free process, roughens topography at all wavelengths. This roughening is balanced by diffusive processes (scaling as $1/L^2$) at short wavelengths and deposition (scaling as $1/L^2$) at long wavelengths. Such a mixture of scale-free and scale-dependent processes can produce multifractal behavior in the models. The fractal dimension of the model topography is much more sensitive to climatic variables than to tectonic uplift. Landscape evolution may be fractal, but it does not seem to be chaotic. Analysis of topography of areas in southern Arizona using variograms shows approximately fractal behavior, with mean fractal dimension around 2.2–2.3. Departures from an exact fractal relationship imply that the topography is in detail multifractal. The fractal dimension at short wavelengths is less than that at long wavelengths. This variation could either be caused by the relative strengths of diffusive and erosional processes shaping the topography, or a result of changes in climatic or tectonic conditions still preserved in the landscape.

Introduction

Recent years have seen an increasing realization that surficial mass redistribution is an important, even crucial feedback element in mountain-building processes (Molnar and Lyon-Caen, 1988; King et al., 1988; Stein et al., 1988; Flemings and Jordan, 1989). Models of large-scale landscape evolution are needed to understand the structural as well as the topographic development of major landforms. In this paper I develop a three-dimensional numerical model of fluvial landsculpting operative over large periods of time and large spatial scales. The model is based on very simple approximations intended to capture the synoptic effects of fluvial processes. If successful, it will allow insight into how the complexity of natural landscapes develops. Experiments with the model also offer tentative insight into how climatic and tectonic variables affect the evolution of landscapes.

The results of the model also relate to the complexity of natural landscape and its description through the language of fractal geometry. Such description is not an end in itself, but may open a path to understanding the interplay of climatic and tectonic influences on the development of landscapes. Fractal analy-

Correspondence to: C.G. Chase, Department of Geosciences, University of Arizona, Tucson, AZ 85721, USA.

sis of some data drawn from a digital topography model of southern Arizona shows that multifractal behavior seen in the models is also characteristic of some natural landscapes. Consideration of the scaling relationships underlying fractal geometry may help construct useful approximations, valid at mountain-range scales, of the laws governing landscape evolution.

A model for fluvial landsculpting

The human race has directly recorded landscape changes over a meager time scale compared to the millions of years that major landscape evolution requires. This is one reason it is desirable to model numerically the long-term and large-scale evolution of topography. With appropriate models we can follow the evolution of one landscape and avoid having to apply the "ergodic principle" (Craig, 1982) of patching together a history from many present-day landscapes we hope are in some sort of developmental sequence. Below I present a three-dimensional model of landscape evolution based on cellular automata (Chase, 1988; Mayer and Chase, 1989; Chase and Mayer, 1989). Using very simple and nearly linear rules for the action of simulated storms, or *precipitons*, we can produce realistic-looking model topographies. The evolution of these model landscapes demonstrates a number of principles readily observable in real landscapes, and suggest some new interpretations as well. As will be discussed in a later section, the model also produces realistic fractal and multifractal geometries, thus establishing that the complexity of landscapes doesn't *require* highly nonlinear processes.

The idea of using simple rules to catch the essence of land-sculpturing processes is not a new one. G.K. Gilbert (1877) enunciated three laws of landscape formation in his classic Henry Mountains report: the law of uniform slope or declivity, by which speedier erosion of steeper slopes tends to reduce the landscape to low relief; the law of structure, by which hard rocks erode less quickly and therefore stand out; and the law of divides, whereby streams steepen toward their headwaters. Because the cellular automaton model presented here also incorporates three principal rules, none of which would have been all that foreign to G.K. Gilbert, the computer program that implements it is named Gilbert in his honor. The model processes employed in Gilbert the computer program produce the three laws of Gilbert the geologist as consequences.

There have been a number of computer-based models for small-scale landscapes (Sprunt, 1972; Ahnert, 1976; Kirkby, 1986), but so far I have seen only one published (Koons, 1989) that specifically addresses mountain range-scale and long-term evolution. Koons' (1989) model provides fascinating insights into the evolution of the Southern Alps of New Zealand, but is based on diffusional transport mechanisms. As we shall see, diffusion alone is not enough to explain landscape.

The use of cellular automata as computational devices has several virtues. A cellular automaton is in effect a set of rules iteratively applied to individual points of a grid of numerical or logical values (Codd, 1968). The automaton has a set of states that evolve according to the values of the cell on which it resides and those of its nearest neighbors (Von Neumann, 1966). The automata used here are slightly unconventional in that they move across the grid of values, just as floods move across a landscape. The rules by which the automaton operates can be as simple or complex as desired, without changing the basis of implementation. This is one definite advantage over a formulation in terms of partial differential equations. Here, I have attempted to reduce the rules to the starkest form of simplicity that can still reproduce some of the complexity of natural landscapes.

The rules governing the cellular automata are in a sense homologous to the natural processes.

Thus the effect of gravity in causing water to almost always run downhill is embodied in the rule that the cellular automata move to lower elevation if they can and stop if they can't. Although the rules governing the automata are minimal, the models still show a very rich variety of behaviors.

The scaling properties of the model are crucial for two reasons. One has to do with relating the results to fractal geometry of landscapes, which describe the scaling of topographic relief. The other is a practical one. If we wish to model both hills and mountain ranges, to make the calculations affordable we must be able to adjust the spatial resolution of the model and obtain equivalent results with both coarse and fine grids.

Precipiton model: general principles

This three-dimensional model of fluvial erosion and deposition is implemented by calculating the cumulative effects of single increments of precipitation (precipitons) that are dropped at random on a digital topography grid, then move downslope, carrying out erosion, transportation, and deposition. The precipiton, as a simple mobile cellular automaton, has the conceptual and computational advantage of handling fluvial transport and deposition as easily as erosion and diffusional slope degradation.

The model is designed to simulate mountain-scale processes on a simplified but actualistic basis, emulating the large-scale effects of fluvial erosion and deposition by merging the overall action of the detailed small-scale geomorphic processes into as few parameters as possible. Three input parameters may be sufficient for many situations. This approach of studying the large-scale and long-term landscape evolution as a whole is akin to studying heat transport or mechanics in physics by dealing with large-scale laws rather than worrying about the motions of individual particles. The processes are almost all non-linear and complicated in action, but their synoptic effect on the landscape may be represented by simpler, nearly linear laws.

There is a stochastic element in the precipiton model, in that the precipitons fall at random on the digital topography. After that, their action is deterministic. Each precipiton represents a single event of precipitation, conceptually that size of event that has the greatest product of probability and geologic action (Wolman and Miller, 1960; Wolman and Gerson, 1978). This might, for instance, be the hundred-year flood, or an even less probable but more catastrophic event.

The model simulates tectonic and isostatic uplift by allowing uplift rates that vary as a function of position on the digital topographic grid. The uplift function can have a separate value for each point of the topographic grid, and the uplift can vary in time in any way desired. At present, only vertical motions are easily implemented.

Before going on to describe the model processes, a few more comments are in order. One is that in a model intended to work at grid resolutions up to km, there is no point in attempting to distinguish between hillslope and channel elements of the topography. Each grid cell represents topography containing both. Therefore, no a-priori distinctions are made between slope and channel, and the rules are uniform for all grid cells. The model must then form its own channels, rather than having them imposed from outside. The rules of the precipiton model produce down-stream convergence of flow in an unforced way. By sending single packets of precipitation through the model at a time, the routing problem for storm flow is avoided. For the model to work with only one precipiton on the grid at a time requires the assumption that the effects of precipitons are linearly independent. The rules adopted here are consistent with independence.

A final comment is that I have found animation of the operation of the model to be both fascinating and educational. To actually see the

model landscapes evolve seems to give extra understanding of the nature of the complex and subtle feedback loops between elevation, slope, erosion, and deposition in the model, if not in nature.

Precipiton model processes and operative rules

The realm in which the precipiton operates is expressed in Fig. 1. The grid of digital topography, with cell dimension L, has no resolvable structure at scales smaller than L. Any behavior a cell has is determined by its single value of elevation (and the elevation of its neighbors), and its material properties, especially erodibility.

Into this grid a precipiton is dropped, say on the cell numbered 1. The first geologic action to be simulated is diffusive smoothing, representing the geologic effects of weathering and mass wasting processes such as slope wash, slumping, talus formation, soil creep, and storms too small to count among the most effective (Table 1). The diffusion is carried out by slope-proportional downhill transport between the target cell and its four nearest neighbors, 3, 5, 7 and 9. Material so transported is given the erodibility characteristics of alluvium. The diffusion is modeled as linear Fickean diffusion, so its transport effectiveness decreases as $1/L^2$. A grid with cells twice as large in L as another will diffuse four times as slowly. The transport coefficient for the diffusion is set proportional to the erodibility of the surface materials, whether alluvial or bedrock. The diffusion pass is done only as each precipiton first falls, so that weathering in the model will be controlled by amount of rainfall. An orographic effect can be simulated by increasing the probability of a precipiton falling at high elevation relative to low. Calculating the diffusion effect at first contact makes "wetter" areas erode faster because more weathering action is included.

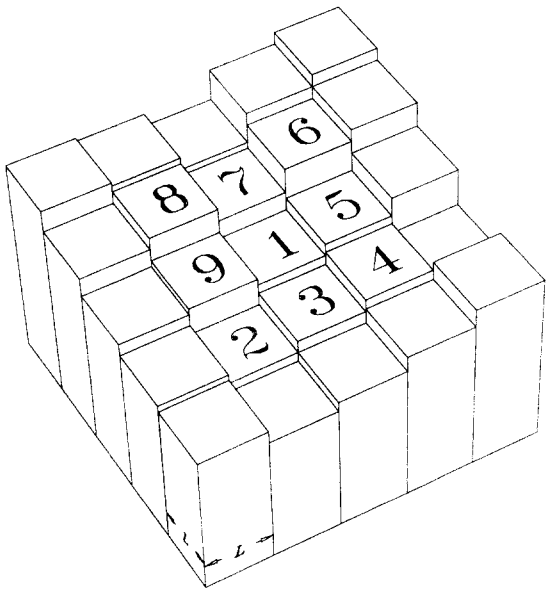

Fig. 1. The world according to the precipiton model. A precipiton is randomly seeded on a digital topographic grid with each grid cell represented by a single elevation. Grid cell size L is shown at the bottom of the figure. A precipiton falling at cell number 1 causes diffusive action on the four nearest cells, here numbers 3, 5, 7 and 9. The precipiton then moves to the lowest adjoining cell, here number 2. It will erode from cell 1 an amount of material proportional to the elevation difference between 1 and 2 multiplied by an erodibility coefficient. Deposition takes place when the precipiton's sediment carrying capacity, proportional to slope, is exceeded.

Having fallen and caused some local diffusion, the precipiton searches for the lowest cell among its eight nearest neighbors, in our present example cell number 2 of Fig. 1. If that cell is lower than its present elevation, the precipiton moves there, and "erodes" material from its original cell (cell 1 here) proportional to the *elevation difference* between the cells and the erodibility coefficient of the material of the original cell. Were no near neighbor lower than cell 1, the precipiton would terminate, dropping any sediment it might be carrying. Material removed by erosion is budgeted to the precipiton as sediment load that it transports downhill. As a precipiton moves away from the cell where it originally fell, it continues to accumulate eroded material if it has not exceeded its sediment carrying capacity.

No adjustment in the erosional process is

TABLE 1

Model processes underlying the rules by which the precipiton model operates, their scaling properties, and generalized relation to climatic parameters

Model process	Represents	Scales as	Climate proxy
Diffusion	Weathering, slope wash, mass wasting, talus, soil creep, small storms	$1/L^2$	Higher values represent more humid, rapid weathering climates
Erosion	Removal of material into suspension or bed load, corrasion	L^0	Climate controls amount of time each storm represents and amount eroded by each storm
Deposition	Sediment carrying capacity proportional to stream power (discharge times slope). When exceeded, deposition occurs	$1/L$	Larger carrying capacity should represent larger storms and more competent floods

made for diagonal distance, or the scale constant L of the grid. This makes the erosion process scale free (Table 1). This is at first surprising, as a slope-dependent erosion function is more attuned to conventional wisdom. However, scaling experiments, a sample of which is displayed in Fig. 2, have shown that for bedrock erosion $1/L$ scaling (inverse slope dependence) makes the model inconsistent when the grid resolution is changed. For a given number of precipitons, the erosion is underestimated when a coarser grid is used to cover the same model feature (Fig. 2). Chris Paola (pers. commun., 1991) has convinced me that $1/L$ scaling would be more appropriate for erosion of sediments, which are transported according to a $1/L$ law. However, this change has not yet been incorporated in the models shown here.

The ability to erode and the transport capacity of the precipiton are limited by a slope-dependent carrying capacity (Table 1). This carrying capacity is an implementation of Bagnold's law (Bagnold, 1966) of sediment transport. The sediment-carrying capacity is proportional to steam power, or slope times discharge. In this model, the precipitons are considered to represent equal, if large, discharge events, so the carrying capacity is left as proportional to slope. When decrease of slope downstream cause a precipiton to exceed its carrying capacity, deposition starts. To prevent infinite loops, deposition is partitioned between the present and previous cell occupied by the precipiton. The amount of deposition is also restrained so that slopes are never directly reversed by deposition. Deposition controlled by slope scales as $1/L$, so that a grid with the same elevations as another but a larger L will experience more deposition for a given precipiton sediment load.

Precipitons terminate when there is nowhere left to go and their sediment load has all been deposited, or when they reach the edge of the grid. They may deposit on the edge of the grid (simulating alluvial buildup) or not (simulating a constant base level) as desired.

Scale and the precipiton model

Figures 3 and 4 explore some of the effects of scale and illustrate the relative effects of the three model processes as they develop over a run of 20,000 model storms. The runs are paired, with both with the same number of cells but one model having L twice as big as the other. All runs start with the initial topography shown center left in the two figures. The mesh

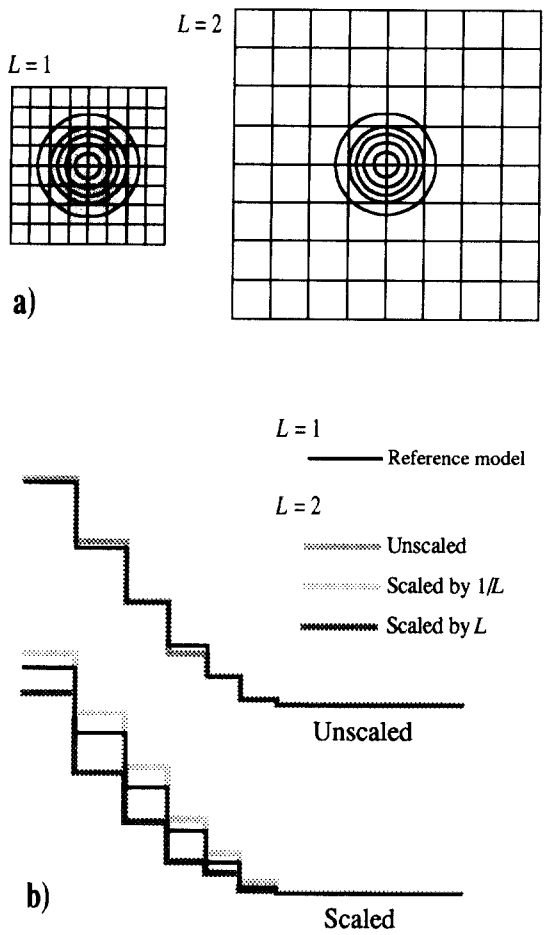

Fig. 2. Numerical experiments showing that the erosional process must scale as L^0 to maintain compatibility of different grid resolutions. (a) The same feature, a conical hill shown by the circular contours, is represented at two different grid resolutions, $L=1$ and $L=2$. (b) Profiles across the conical feature averaged as a function of radius after 20,000 model storms, vertical exaggeration 7.5 to 1. The upper profile compares the reference model ($L=1$) with an unscaled $L=2$ model (erosion proportional to elevation difference, or L^0 scaling). The upper profile displays an acceptable fit, in contrast to the lower profile showing the effect of erosion proportional to slope ($1/L$ scaling) and for L^1 scaling in the $L=2$ models.

plots in Fig. 3 are vertically exaggerated but show relative horizontal scale, while in the contour plots of Fig. 4 the large- and small-model areas are shown the same size to make comparison easier. Contours to scale for one model (all processes operative) are displayed in Fig. 5. The starting model represents a conical volcano with an eccentric crater.

The height is the same for both large- and small-area models (Figs. 3 and 4), so the slopes are steeper for the small-area models. The small-area models ($L=1$) represent topography of the same amplitude but shorter wavelength than the $L=2$ models.

To describe quantitatively the effects of the various processes on the complexity of the model landscapes, I will use the mean fractal dimension D. How I estimate the fractal dimension and more details of what it means are discussed in subsequent sections. For the moment, it suffices to note that a surface with a fractal dimension of 2.0 is very smooth and plane-like. At low values of D near 2.0 the elevations of nearby points correlate very strongly, while points separated by large distances have greater variability in elevation. As D becomes larger, the variability of elevation for nearby points becomes more similar to that of distant points. At $D=3.0$ the surface is so rough that adjacent and far points are completely uncorrelated in elevation, and the surface in essence becomes space filling. In this view, the fractal dimension is a measure of surface complexity, and high D represents high complexity. Fractal dimension is independent of amplitude of relief on the surface. The fractal dimension of the initial topography in Figs. 3 and 4 is 2.11. This represents a fairly smooth surface.

The models using diffusion alone (lower left, Figs. 3 and 4) show the strongest effect of scale. The $1/L^2$ scaling causes the diffusion to be a very effective smoothing agent for short distances, but quadratically less so as the length scale increases. This is reflected in reduction of the fractal dimension for the small-area model to 2.02, while the large-area model is reduced to 2.06 from the original 2.11. The difference is clearly visible in the contour plot at lower left of Fig. 4.

The pure erosion models (upper left, Figs. 3 and 4) show no effects of scale, as advertised. The contours are identical. For both, the fractal dimension has been raised to 2.50, and con-

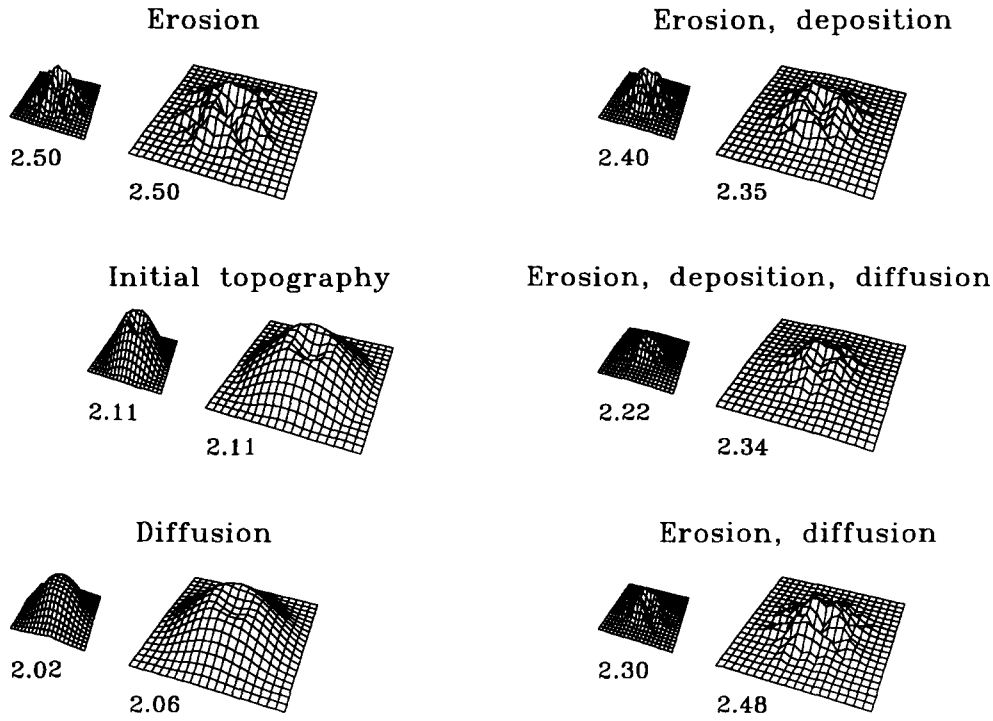

Fig. 3. Perspective mesh diagram showing the effects of combinations of the precipiton model processes on an initial topography representing a conical volcano with an eccentric crater. Large (long wavelength, i.e., $L=2$) and small, (short wavelength, $L=1$) versions of the same model were run for 20,000 storms each .The small version of the initial topography has the same model height as the large version, so the slopes are steeper in the small versions. The numbers below each model are the mean fractal dimension as measured from variograms.

tinues to rise if the model is run longer. As a scale-free process, erosion in the precipiton model roughens the landscape at all scales equally. In as far as landscape is fractal, some such process must dominate. The lack of a roughening process is also the reason why diffusion-based models cannot properly simulate the evolution of landscapes. Koons' (1989) model for the Southern Alps of New Zealand required the artificial introduction of controlled stream drainages and profiles, because diffusional models can't develop drainage on their own.

The frames on the right in Figs. 3 and 4 show the effect of combined processes. Deposition can't be shown by itself, as there would be no source of material for the precipitons to transport. The general conclusion that can be drawn from comparing the models on the right is that the depositional process smooths at long wavelengths. For erosion and deposition together (upper right) the large-area model has a lower fractal dimension (2.35) than the small (2.40). However, when diffusion is added so that all processes are active, the small area becomes smoother, with D equal 2.22 as compared to 2.34 for the large-area model.

The overall picture that emerges is that these model topographies are approximately fractal because the erosional process roughens at all scales, while the diffusion process smooths the topography at small scales and the depositional process smooths it at large scales. Something like this is probably also true of natural landscapes. A secondary conclusion from these results, maybe even a prediction, is that small hill should be smoother than large hills, even if they start with steeper slopes. This can be seen

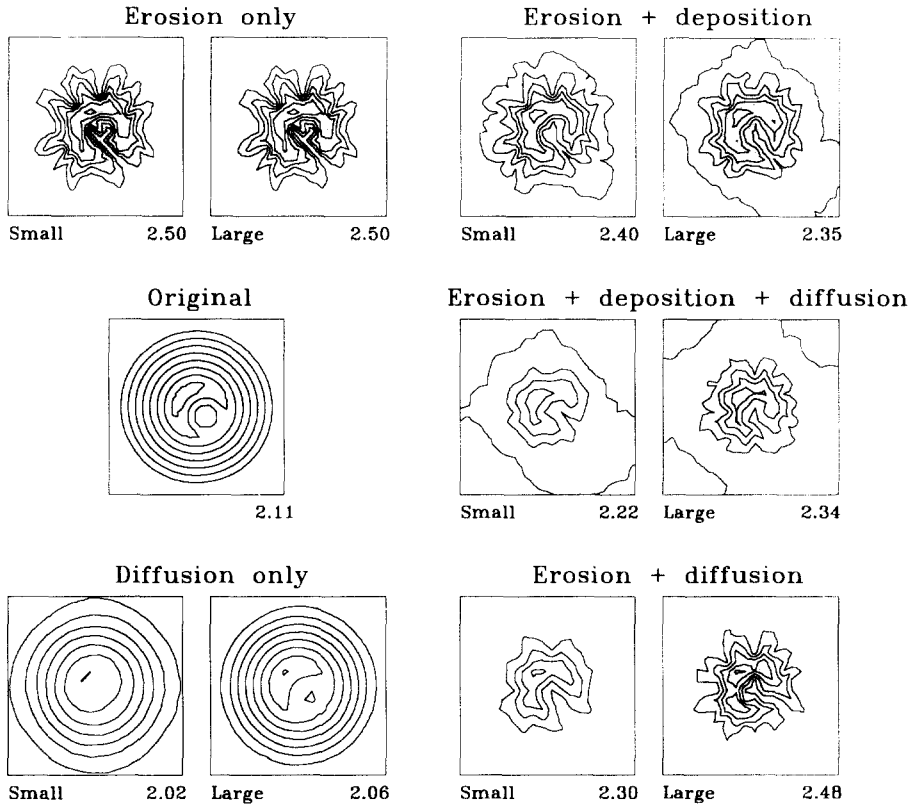

Fig. 4. The same suite of models as Fig. 3, only represented in contour form. The contour maps of the large ($L=2$) models are reduced by a factor or two for direct comparability with the small ($L=1$) models. See Fig. 5 for an correct scale rendition of one model. Contour interval somewhat arbitrary but constant for all models, intended to be something like 250 m.

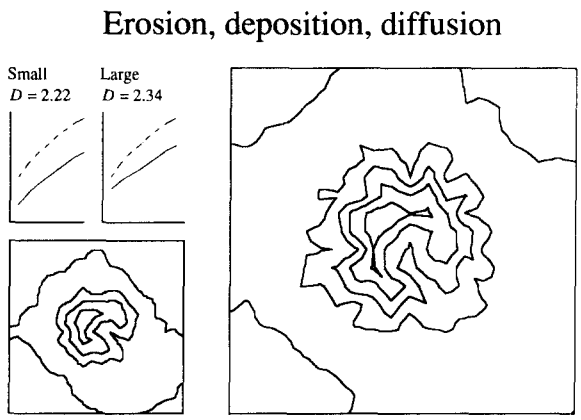

Fig. 5. One pair of models, with all processes operative, and contour maps plotted to true relative scale. The inset shows the variograms for the large and small models, with the dash-dot line marking the variogram of the initial topography.

by comparing the large- and small-area plots of Fig. 5. I cannot claim to have made an exhaustive study of small hills versus large hills, but at least anecdotal evidence from topographic maps and the scenery of southern Arizona is consistent with the prediction.

Climate, tectonics, and the precipiton model

The erodibility of model materials, the ratio of diffusive action to erosive action, and the sediment carrying capacity are all to some extent proxies for climatic variables (Table 1). Imposed uplift is the proxy for tectonic effects. It is clear that these variables control the model landscape evolution, but it is not necessarily easy to relate the climatic proxies to what is conventionally thought of as climatic controls.

The erodibility of the model rocks can be stratigraphically layered and optionally, those layers can be warped vertically in the present implementation of the program Gilbert. In addition "alluvial" materials deposited in the model can be assigned a separate, usually higher erodibility. In effect, setting the erodibility of the rocks is an important component of establishing the time scale of the model. One external observable, or at least guessable, to which the model clock can be calibrated is the rate of denudation of the landscape. The higher the erodibilities are set, the faster time passes per precipiton by this standard. The other possible calibration, as discussed above, is through definition of recurrence interval of the most significant storm event. Both need be considered for a consistent time scaling. In general, however, for the same time per precipiton, higher erodibilities will probably correspond to more chemically and physically aggressive climates. Material must be physically or chemically weathered before it can be removed.

The relative importance of diffusive redistribution compared to erosive removal of material is another climatic proxy. High rates of diffusive activity correspond to rapid mass wasting, slope, wash, soil creep, and slumping. Humid climates should experience relatively more of these kinds of diffusive processes than dry ones. Figure 6 displays the results of model runs varying the ratio of diffusive to erosive activity (d/e) and the horizontal scale L of the models. The upper part of the plot shows the effect on average fractal dimension. The "dry" ($d/e=0.1$) models are relatively insensitive to scale, while the "wet" models clearly show the greater effectiveness of diffusive smoothing at short wavelengths. This implies that below some threshold, diffusive action becomes unimportant in controlling the average fractal dimension.

Figure 6 also shows the effect of d/e and scale on peak and mean elevation of the model landscape during its evolution. The average elevation responds more to scale than to "wet" or

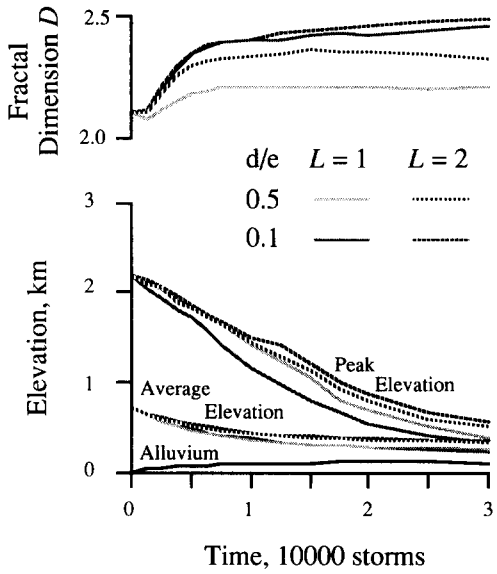

Fig. 6. The effect of ratio of diffusional to erosional processes (d/e) on the evolution of model topography. Initial topography same as shown in Fig. 3 and 4. Four models, long ($L=2$) and short ($L=1$) wavelength coupled with high (0.5) and low (0.1) ratio of diffusivities to erodibilities, are shown. The carrying capacity for these models was 1.0. The buildup of alluvial thickness for all four was similar enough to represent with a single curve.

"dry" conditions, while alluvial thickness is insensitive. Only in peak elevation is there much of a difference related to diffusive action. This demonstrates that diffusion is not an effective long-distance transport mechanism in any of these models.

The sediment-carrying capacity of the precipitons is also a climatic proxy variable, as well as part of the time-scaling question. Large carrying capacities represent conditions under which the most effective storms cause very large floods. This is related less to total amount of precipitation than to how it is distributed in time. A mostly arid desert with a very large 100-year flood might require higher carrying capacity than a tropical region with much more annual precipitation. In the limit, as the carrying capacity approaches zero, the action of the erosive/depositional process approaches linear diffusion. In effect, the precipiton decouples the erosional and the depositional parts

of what would otherwise be a diffusive process, and allows material to be carried rapidly to large distances.

The effects of carrying capacity change do not show the threshold of indifference to scale that was characteristic of the diffusion/erosion ratio. As seen in Fig. 7, higher carrying capacities are more erosive and favor larger fractal dimensions for both long- and short-wavelength models. The long-wavelength models show somewhat stronger sensitivity to carrying capacity. Dispersion in the denudation rates for these models is more marked than those of Fig. 6, as might be expected. The main means of transport is being adjusted, and both peak and average elevations respond to the changes. Feedback in the models keeps the responses from behaving linearly, however. Note that the average elevation at 30,000 storms for the $L=2$ models is only halved while the carrying capacity is increased by a factor of four.

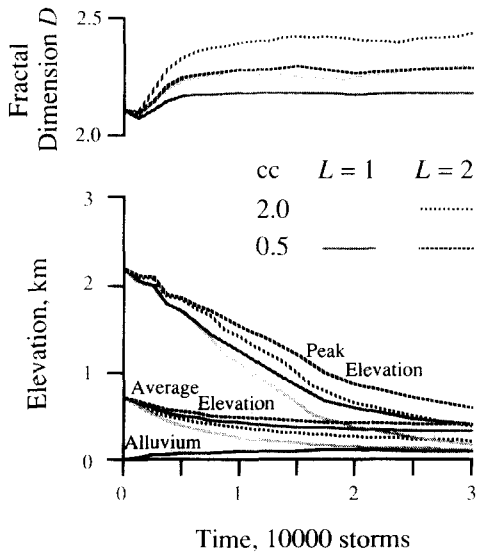

Fig. 7. The effect of carrying capacity variation on evolution of model topography. Initial topography same as shown in Figs. 3 and 4. Four models, large and small size coupled with high (2.0) and low (0.5) sediment carrying capacity (*cc*) coefficients, are shown. The diffusion/erosion ratio for these models is 0.5. The buildup of alluvial thickness for all four was similar enough to represent with a single curve.

At $L=1$ the residual elevation at the end of the run is more commensurate with the carrying capacities. One conclusion from this set of runs is that maximum effective storm size (proxied by carrying capacity) is an important, perhaps the most important climatic variable in determining the landforms that develop.

The final numerical experiment I will deal with here attacks the problem of how tectonic activity affects the model fractal dimension. For this purpose, a model was run for 30,000 storms with extremely active uplift of a "boxcar" shaped block across the span of the grid (Fig. 8, left). Then, without changing any of the climatic parameters, the uplift was stopped, and the model allowed to erode for another 30,000 storms (Fig. 8, right). The model topographies at these stopping points, plotted to the same contour interval in Fig. 8, are conspicuously different. During the uplift, the fractal dimension reached some sort of steady state (Fig. 9), then actually rose slightly when the uplift stopped. This is not encouraging in terms of identifying high fractal dimension with tectonically active areas. In fact, the result is understandable in terms of the relationship of fractal dimension to roughness variation with scale. The tectonic uplift feeds information into the topography at long wavelengths only, thus tending to make the variogram slightly steeper. When this tectonic input ceases, the fractal dimension rises to its climatically controlled value. The whole question of relation of fractal dimension to tectonic activity is examined, using real data, in the companion paper by Lifton and Chase (1992 – this issue).

Precipiton discussion

The complicated topographies produced by the Gilbert models (Figs. 3, 4 and 8) demonstrate one thing clearly: a complex landscape does not *require* complex rules. Natural landscapes may indeed be formed by inextricably non-linear and difficult processes, but the re-

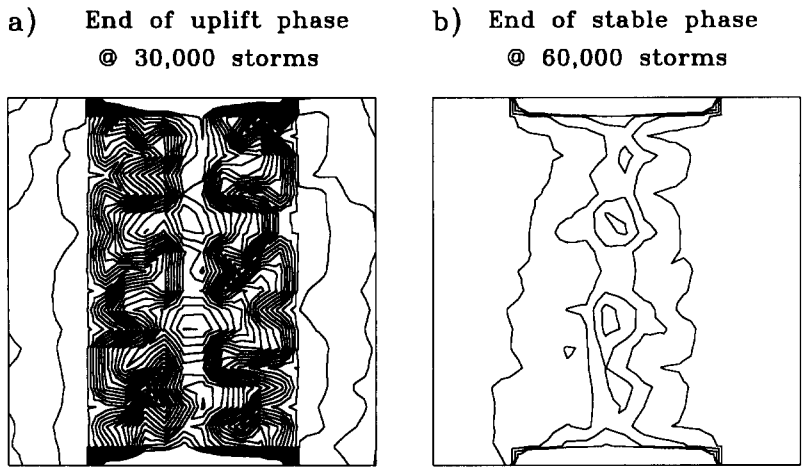

Fig. 8. Contours of model sequence showing indifference of fractal dimension to rate of tectonic activity. (a) Contours of model topography after 30,000 storms falling on vigorous, active uplift with rectangular cross section. (b) Situation 30,000 storms after uplift is stopped. All erosional parameters except uplift rate the same as in (a). Contour interval same as for (a).

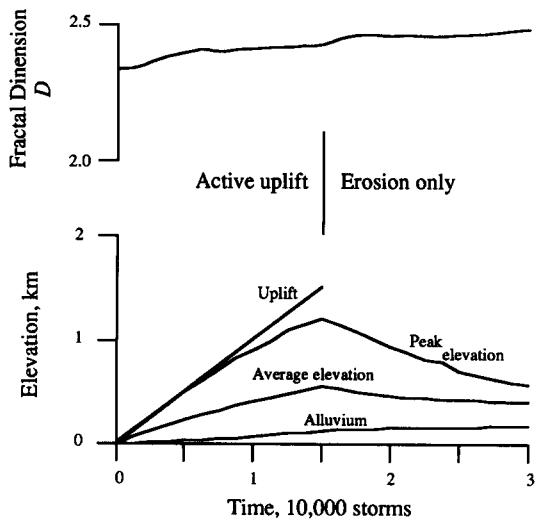

Fig. 9. Evolution of fractal dimension D, peak and average elevation, and alluvial thickness for model shown in Fig. 8. 30,000 storms of rapid uplift are followed by 30,000 storms with no uplift, all other erosional parameters held constant.

sults of these models offer some hope of understanding landscape evolution in terms of simpler, synoptic generalities. The feedback loops between the form of the landscape and the processes that excavate and transport material across it may be more important than the actual details of those processes.

Accepting the general outlines of this model, then the approximately fractal geometry of natural landscapes is forged in the balance between roughening at all scales by erosive processes and smoothing at small scales by diffusive processes augmented with smoothing at large scales by depositional processes. This conclusion is robust to the details of the processes and how they are simulated. Delving into more model-dependent conclusions, the point of balance and the degree of landscape complexity is much more responsive to climatic influences than to tectonic ones. Of course, the amplitude of relief is much more immediately controlled by the level of tectonic activity.

If I might be permitted a few speculations, prejudices and observations acquired by hours of watching these model landscapes evolve: the development of fluvial topography may lead to fractal geometry but it is not chaotic. Initial conditions for the model topographies that are close together lead to final models that resemble each other strongly. This is certainly true for the erosive part of the model, but might not be as true for the depositional part, were one to label the deposited material with its point of origin. Inheritance in the model landscapes is strong, and a die cast early can be seen stamped

on the final product. Notice in Figs. 3 and 4 that the eccentric crater of the initial topography lives on in the U-shaped high parts of the eroded models. Once one part of the landscape has an advantage in drainage area, it keeps ahead of the rest. Among its rich repertoire of behaviors, Gilbert makes pediments readily where eroding mountain cores grade into stable alluvial aprons. Only under these circumstances does lateral planation occur easily. Where precipitation falls is important, as precipitons from the headwaters of drainage systems come through laden with sediment and in a depositional mode, while precipitons falling lower in the system are unladen and thereby highly erosive. Partly because of this balance between traveled and fresh precipitons, the grade or profile of the model rivers is one of the characteristics most sensitive to all the parameters, and therefore should be a focus point for calibration of the models against real landscapes.

In the next section I will flesh out how the fractal dimension of the model landscapes was determined, and offer some data on actual landscapes for comparison with model results. This will involve going beyond strictly fractal behavior.

Complexity and the fractal geometry of landscapes

The complexity of landscapes is one of their most obvious characteristics. Large valleys have smaller tributaries, these in turn are fed by creeks, which collect the product of an indefinite number of rills. Not only are landforms thus nested in scale, but there is a sense of sameness of the features as scale changes. It is not easy to tell from an unlabeled map of drainages whether one is looking at m or km of ground. Alluvial fans 10 km wide formed at mountain fronts closely resemble those 1 m wide formed in road cuts. None of these features are even statistically self-similar, because the vertical scale does not vary the same way the horizontal scale does. They are, however, statistically self-affine (Huang and Turcotte, 1989; Turcotte, 1991).

The complexity of natural landscapes may reflect an underlying order, and it is important in understanding the evolution of landscapes to ascertain if that order exists, and if so, how it arises. It may contain retrodictive and predictive power concerning the tectonic and climatic influences that shape natural landscapes. Because the order is one of scaling relationships, it can give insight into the appropriate nature of the laws governing landscape development at large scales, and guide the construction of conceptual and numerical models embodying approximations to those laws.

For the purposes here of investigating the complexity of landscapes at horizontal scales up to tens of km, it is more appropriate to work with a digital approximation of the topography rather than that of the drainage network it defines. With minimum resolutions of the order of hundreds of meters or of km, there is no part of the system that is not a mixture of hillslopes and channels. At these scales, drainage density is not a particularly useful concept.

The use of the fractal dimension as a descriptor of the complexity of surfaces has been made popular by the efforts of Mandelbrot (1982, for review of his publications). A surface can vary in its texture from extremely smooth, which would represent a fractal dimension of 2, the same as its Euclidean dimension, to extremely complex, and jagged, so that it becomes in some sense space filling. This latter surface would have a fractal dimension approaching 3. The fractal dimension of a surface, as noted before, is independent of the amplitude of its relief. Likewise, curves may have fractal dimensions between 1 and 2. Any intermediate value is possible. In general, the surface fractal dimension should be greater by one than the fractal dimension of a profile or contour of that surface (Mandelbrot, 1982; Voss, 1988).

Many environmental variables seem to be fractal (Burrough, 1981; Mandelbrot, 1982). To be a true fractal, a topographic surface needs to be at least statistically self-affine, so that it looks about the same represented at any horizontal scale. In approximately fractal surfaces, this size independence may be restricted to a limited range of scales. Natural topography approximates a fractal with dimension usually between 2.1 (smoothish) and 2.7 (rugged indeed) (Burrough, 1981; Mandelbrot, 1982). Obviously, if we deal with discrete digital topographic data, the smallest scale available is limited to the grid spacing and the largest to the area covered by the data set.

Natural landscapes are often only approximately fractal, and show apparent fractal dimensions that change as a function of horizontal distance (Culling and Datko, 1987; L.E. Gilbert, 1989; Goodchild, 1980; Mark and Aronson, 1984; Chase and Woodward, 1990). Mark and Aronson (1984) found that some areas demonstrate variable fractal dimensions over different scale ranges. In particular, data from several quadrangles in Pennsylvania showed fractal dimension D of 2.2 at scales smaller than 0.6 km and D from 2.5 to 2.75 at scales between 0.6 and 5 km. Such a variation of apparent fractal dimension as horizontal length varies can be described as multifractal behavior (Mandelbrot, 1989). A multifractal surface will have a different characteristic fractal dimension at different horizontal wavelengths. Most of the data from the semiarid Southwest presented here is discernibly multifractal. Roy et al. (1987) suggest that this apparent multifractal nature may be due to anisotropy in the topography at long wavelengths. The data shown here is chosen in a way that should minimize anisotropic effects.

Variogram technique

I have chosen here to investigate the complexity of natural landscapes using the fractal dimension of the topographic surface as determined by the variogram method (Mark and Aronson, 1984). This method has proved to me rather more intuitive than other ways of estimating the fractal dimension, such as Fourier spectra (Huang and Turcotte, 1989; L.E. Gilbert, 1989; Turcotte, 1991). Variograms sometimes give different results than other methods (Clarke and Schweizer, 1991). However, we are using the same measure to compare both model and natural landscapes, so it doesn't particularly matter what the "true" fractal dimension is, only how the same statistical measure of complexity compares for both.

The variogram of a surface is constructed by considering the variance of its elevation as a function of horizontal distance. For a pair of points x_1, y_1, z_1 and x_2, y_2, z_2 on a grid of digital topography with x and y horizontal coordinates and z the elevation, the contribution to the variance is $(z_1-z_2)^2=(\Delta z)^2$ and the horizontal distance is $[(x_1-x_2)^2+(y_1-y_2)^2]^{1/2}=\Delta x$ (see Fig. 10). We calculate these for every pair of points on the grid, and plot the logarithm of the standard deviation over a binned distance interval against the logarithm of the distance at the logarithmic midpoint of that

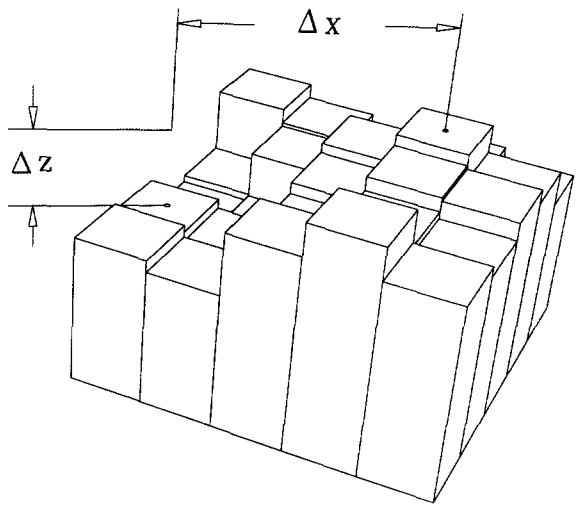

Fig. 10. Geometric basis for the calculation of variograms. The topographic variability is given by the average of the elevation difference Δz. This is then plotted as a function of (binned) horizontal distance Δx.

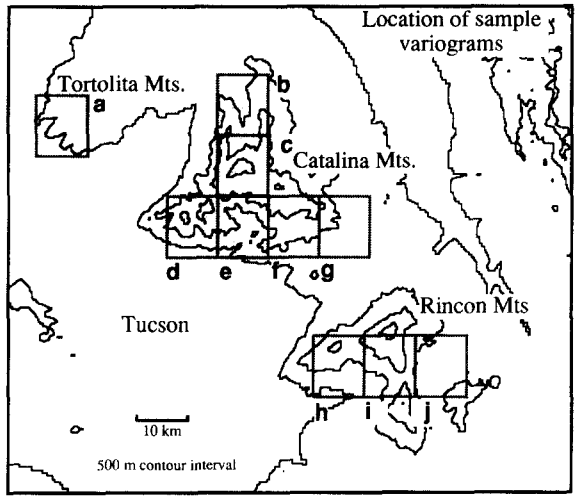

Fig. 11. Location map of mountains surrounding Tucson, Arizona. The shaded boxes represent the approximately 10-km-square regions from which the variograms of Fig. 12 are drawn. Elevations from 15 second digital topographic data set. Contour interval is 500 m, and the lowest contour is at 1 km elevation.

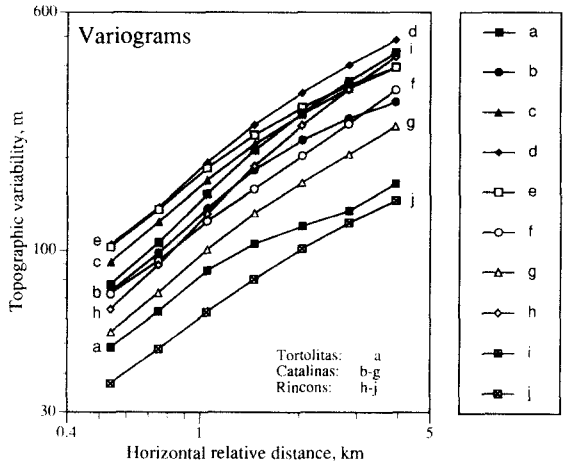

Fig. 12. Variograms for the ten areas identified in Fig. 11. Topographic variability in m is plotted versus horizontal distance in km. Distance bins are at equal logarithmic intervals. Note that the variograms approximate straight lines (fractals) with varying degrees of success.

interval. This is a computationally intensive operation, because an n by n grid contains $n^2(n^2-1)/2$ point pairs.

A convenient sample (for me) of natural topography is drawn from a digital elevation model of southern Arizona. Figure 11 shows the location of several 20 by 20 point grids (9.3 north–south by 7.8 km east–west) of digital topography drawn from U.S. Geological Survey 15 second data. In this data set, the grid cells are approximately 460 m tall (north–south) and 390 m wide (east–west). No attempt was made to correct for the map distortion. The areas are chosen to represent mountainous regions with a variety of total relief. The shortest length scale represented is the grid spacing, while the longest has been clipped to half the total grid size to avoid sampling problems. Roy et al. (1987) suggest an even shorter cutoff, but these small data sets would have almost nothing left. Thus wavelengths between 460 m and 4.6 km are present. Figure 12 contains the resulting variograms. The distance bins have been chosen at logarithmically equal intervals.

The relationship of the variogram to surface fractal dimension is straightforward. For a three-dimensional, self-affine fractional Brownian function (Voss, 1988, eq. 1.8), which is characterized by a single fractal dimension:

$$\langle (z_1 - z_2)^2 \rangle = K[(x_1 - x_2)^2 + (y_1 - y_2)^2]^{(3-D)} \quad (1)$$

where the angle brackets $\langle\ \rangle$ represent an average over the binning interval, K is a constant that scales horizontal to vertical variation, and D is the fractal dimension. Equation (1) implies that on a logarithmic plot of standard deviation versus distance (Fig. 12), the slope of the variogram is $(3\text{-}D)/2$. Thus a steeply sloping variogram represents a low fractal dimension, and a shallow slope represents a high fractal dimension.

Because of this relationship to slope of topographic variance, the fractal dimension of topography is controlled by how its variability changes with distance, not the amplitude of that variability. A high fractal dimension represents topography that is uncorrelated at all length scales, while a low fractal dimension represents topography that is strongly corre-

TABLE 2

Mean fractal dimension for the ten sample areas, and the r^2 goodness of fit parameter for a least-squares linear fit to the data. Locations shown in Fig. 2 and variograms in Fig. 3. The relief is interpolated on the variograms at 1 km horizontal relative distance

Location	Number	Mean fractal dimension D	Goodness of fit r^2	Relief at 1 km wavelength (m)
Tortolitas	a	2.40	0.973	82
Catalinas	b	2.26	0.975	130
	c	2.25	0.986	163
	d	2.20	0.991	190
	e	2.31	0.980	181
	f	2.22	0.999	120
Rincons	g	2.22	0.993	97
	h	2.02	0.994	128
	i	2.10	0.992	147
	j	2.30	0.993	60

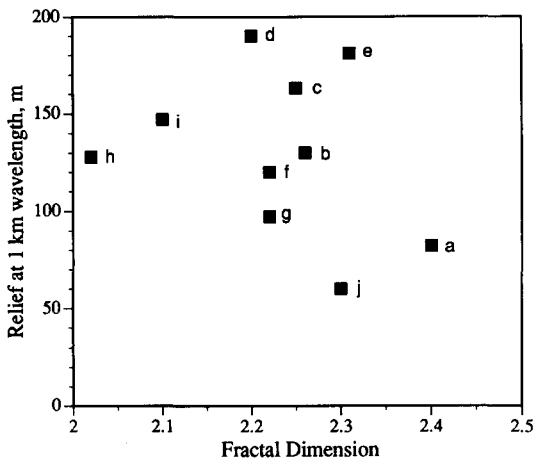

Fig. 13. Relief amplitude estimated at 1 km length scale from variograms in Fig. 12 compared to mean fractal dimension estimated by straight-line fit to entire variogram. Areas keyed by letters to Fig. 11.

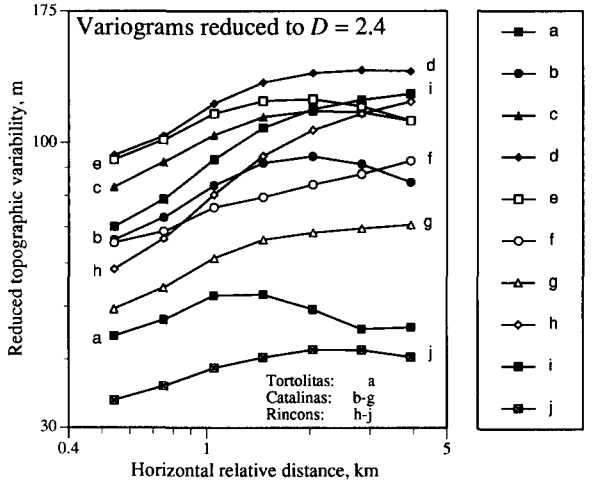

Fig. 14. Variograms from Fig. 12 reduced to fractal dimension $D=2.4$ by subtracting straight line of slope +0.6. Lines on this diagram with positive slope represent D less than 2.4, while lines with negative slope represent D higher than 2.4. Note that most of the variograms are significantly curved, showing multifractal behavior. At wavelengths longer than 1.5 km, the average fractal dimension is around 2.4, while at shorter wavelengths the fractal dimension is less in all cases.

lated at short wavelengths and less so at long wavelengths. The amplitude of the variability, a parameter related to the relief (Huang and Turcotte, 1989), is given by the vertical placement of the variogram. This can be seen in Fig. 12: variograms d and g have quite similar average fractal dimensions, but the relief of region d is almost twice that of region g (Table 2). The average fractal dimensions given in Table 2 are obtained by a least-squares straight-line fit to the variograms. I have quantified the relief by the variability value interpolated on the actual variogram at 1 km horizontal distance. There is no uniform relationship between the fractal dimension and the estimation of relief amplitude (Fig. 13).

A true fractal would have a straight variogram. Although the goodness of fit for straight lines fitted to these variograms is quite high

(Table 2), most of them depart systematically from straightness, and thus are multifractal (Mandelbrot, 1989). Typically, the variograms have steeper slopes at shorter length scales with fractal dimensions around 2.2, and flatter slopes at wavelengths longer than 1 km, representing D in the vicinity of 2.4. This kind of variation is consistent with that reported by Mark and Aronson (1984) for several regions, and by L.E. Gilbert (1989) for a single profile across the Sierra Nevada. To point up the variation in slope, I follow L.E. Gilbert (1989) in plotting a "reduced" version of the variograms in Fig. 14. In this plot, a line of slope equivalent to $D=2.4$ is subtracted from each variogram, so portions of variograms with positive slopes have fractal dimension less than 2.4. For a fractal dimension greater than 2.4, the variogram will have a negative (downward) slope.

Fractal analysis of mountains of southern Arizona

Some of the idiosyncrasies of fractal investigation of real topography are revealed by a closer examination of specific cases. The most crooked of the variograms in Figs. 12 and 14 is drawn from the Tortolita Mountains (Fig. 11), a low satellite range with 0.5 km relief to the west of the higher Catalina range, which has almost 2 km relief. It has the highest average D of any of the data sets here, and the second lowest relief. The fractal dimension D is 2.1 for wavelengths less than 1.5 km, while at longer length scales D approaches 2.6. This particular data set covers both low mountains and a significant portion of alluvial fan and plain. Numerical experiments involving shifting the origin of the data set demonstrate that the mixture of geographic environments encourages the non-linearity in the variogram. This is a sensible result, for the alluvial plain has less absolute variance at long wavelengths. Variograms do not combine linearly: the variograms for a pure alluvial environment and for the hills alone are both uncomplicated, though the alluvial region has lower D and considerably less amplitude of relief.

The variograms for the Catalinas (b–g, Figs. 11, 12 and 14) are rather more linear. The northernmost, b, resembles the Tortolita data set in having a significant mixture of alluvial fan, and likewise a high fractal dimension at long length scales (Fig. 14); c, d and g all have short-wavelength D near 2.1, and long-wavelength D around 2.4. Sample f is the closest of any of these data sets to a true fractal over the range of wavelengths studied. The important things in common among the Catalina variograms are: mean fractal dimension between 2.2 and 2.3; and fractal dimension increasing with length scale.

The three data blocks drawn from the Rincon Mountains (Fig. 11) present one interesting anomaly. The westernmost data block, h, has the lowest fractal dimension of all, 2.02 (Table 1). This is almost as low as it can go and still be a surface. Examination of U.S. Geological Survey topographic maps reveals that most of the topographic roughness in the area has wavelength less than 400 m. The smoothness of this terrain at longer wavelengths is partly due to lithology and partly to structural control, with resistant mylonites forming a dip slope over much of the block. In this case, 15 second topographic data just hasn't fine enough resolution to catch the actual roughness of the area. At the shortest length scales, block i shares the low fractal dimension of h.

Implications of fractal character

The strongest conclusion of this fractal analysis is that the topography of some selected mountain ranges (Fig. 11) in southern Arizona is approximately fractal, with variograms for length scales between 460 m and 4.6 km that show an orderly progression of increasing variance as wavelength increases (Fig. 12). This is consistent with the findings of other workers. The mean fractal dimension from these

variograms varies from 2.02 to 2.40, with an average of 2.22 (Table 2). The fractal dimension D is not a function of relief (Fig. 13).

The second strongest conclusion is that the topography is actually multifractal, and is smoother at smaller length scales within the wavelength range studied (Fig. 14). For length scales between 460 m and 1.5 km, the average fractal dimension is around 2.1, while for length scales between 1.5 and 4.6 km the average D is 2.5.

There are several ways in which the multifractal nature of the real landscape might arise. It may be an inherent result of the laws governing evolution of the landscape at present, or it may in part result from climatic and tectonic changes that have affected that evolution in the past. Woodward (1990) has shown that dissected fans along the northwest side of the Catalina Mountains (area d, Fig. 11) result from base-level or climatic change rather than tectonic activity. Curvature of the variograms could thus be related to transition with time

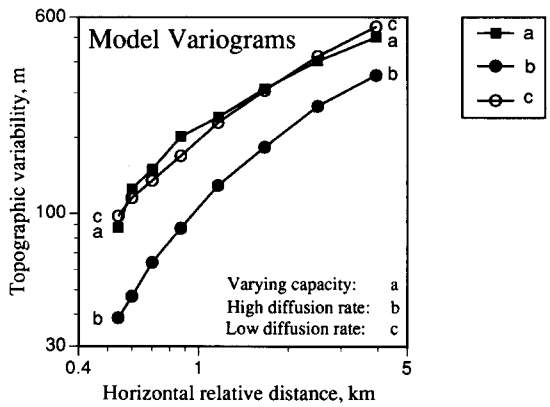

Fig. 15. Model variograms showing several ways to achieve multifractal behavior like that seen in measured variograms (Figs. 12 and 14). a=model run 30,000 storms with low diffusion/erosion ratio, alternating high (2.0) and low (0.1) carrying capacities at 5,000 storm intervals; b=model run with high ratio of diffusive to erosive action, which produces strongly multifractal variogram. This is the case d/e=0.5, L=2, 30,000 storms of Fig. 6; c=low ratio of diffusion to erosion produces more nearly linear variogram: d/e=0.1, L=2, 30,000 storms of Fig. 6. These three models are scaled to relief similar to the southern Arizona samples.

from regimes of relative smoothing of topography to relative roughening, with effects at different length scales having different responses delays. This scenario can be studied with the help of Gilbert. In Fig. 15, the curve labelled "a" represents the variogram from a model run with alternating large and small carrying capacities. The short-wavelength topography is smoothed because, as mentioned above, the precipitons with small carrying capacity act more diffusively than precipitons with large carrying capacity. The result is a multifractal model topography.

Another set of models (Fig. 15; b,c) demonstrate that the balance between diffusive and erosional processes can affect how curved the variogram is, and therefore how multifractal the topography. Variograms from the L=2 models of Fig. 6 show much more curvature for case (b) in which a high diffusion to erosion ratio is used than for a low ratio (a). In fact, the high-diffusion case shows more curvature than any of the variograms measured on real topography. The difference between short- and long-wavelength fractal dimension of natural topographic variograms can thus be used to quantify the relative importance of diffusive versus erosive processes on the landscape.

Summary

A simple but powerful model of landscape evolution based on cellular automata can simulate the effects of diffusive (mass wasting) processes, erosion, and deposition. Each of these processes react differently to changes in horizontal scale. The model produces complex, almost fractal topographies with its simple, almost linear rules. This demonstrates that complex landscapes do not require complicated laws for their formation. The fractal geometry of the models arises from the balance between erosional roughening at all scales and diffusive smoothing at short wavelengths plus depositional smoothing at long wavelengths. The fractal dimension of the models is much

more responsive to climatic variables than to tectonic uplift.

Variograms from selected areas from southern Arizona show that the topography at length scales from 460 m to 4.6 km is approximately fractal, with mean fractal dimension around 2.2–2.3. The systematic departures from an exact fractal relationship imply that the topography is in detail multifractal, with lower fractal dimension at wavelengths less than 1.5 km than for longer length scales. Model results show that this curvature of the variograms could either be inherent to the relative importance of diffusional and erosional processes shaping the topography, or a result of changes in climatic or tectonic conditions still preserved in the landscape.

Acknowledgements

Discussions with many people have helped me develop these concepts and the precipiton model, although they cannot be held accountable for the way it turned out. I wish to thank Kirk Vincent, Larry Mayer, William Bull, Nat Lifton, Julie Woodward, Chris Paola, Andy Cohen and Michael Kirkby for advice and criticism. Especially I thank Don Turcotte for the random spark that started this whole investigation. The manuscript was improved by helpful comments from Kate Gregory, Larry Mayer, Julie Woodward, and two anonymous reviewers. This work was supported by NASA's Innovative Research Program.

References

Ahnert, F., 1976. Brief description of a comprehensive three-dimensional process-response model of landform development. Z. Geomorph., Suppl., 25: 29–49.

Bagnold, R.A., 1966. An approach to the sediment transport problem from general physics. U.S. Geol. Surv. Prof. Pap., 422-I, 37 pp.

Burrough, P.A., 1981. Fractal dimensions of landscapes and other environmental data. Nature, 294: 240–242.

Chase, C.G., 1988. Fluvial landsculpting and the fractal dimension of topography. EOS, Trans. Am. Geophys. Union, 69: 1207.

Chase, C.G. and Mayer, L., 1989. Fluvial landsculpting: Why topography is like a fractal. Geol. Soc. Am., Abstr. with Programs, 21: A39.

Chase, C.G. and Woodward, J.A., 1990. Multifractal topography and climatic history of southern Arizona. Geol. Soc. Am. Abstr. with Programs, 22: A14.

Clarke, K.C. and Schweizer, D.M., 1991. Measuring the fractal dimension of natural surfaces using a robust fractal estimator. Cartogr. Geogr. Inf. Syst., 18: 37–47.

Codd, E.F., 1968. Cellular Automata. ACM Monograph Series. Academic Press, New York, N.Y., 122 pp.

Craig, R.G., 1982. The ergodic principle in erosional models. In: C. Thorn (Editor), Space and Time in Geomorphology. Binghampton Symp. in Geomorph., Int. Ser. 12, George Allen and Unwin, London, pp. 81–115.

Culling, W.E.H. and Datko, M., 1987. The fractal geometry of the soil-covered landscape. Earth Surf. Processes Landforms, 12: 369–385.

Flemings, P.B. and Jordan, T.E., 1989. A synthetic stratigraphic model of foreland basin development. J. Geophys. Res., 94: 3851–3866.

Gilbert, G.K., 1877. Report on the Geology of the Henry Mountains. U.S. Geographical and Geological Survey of the Rocky Mountains Region, Government Printing Office, Washington, D.C., 160 pp.

Gilbert, L.E., 1989. Are topographic data sets fractal? Pure Appl. Geophys., 131: 241–254.

Goodchild, M.F., 1980. Fractals and the accuracy of geographical measures. Math. Geol., 12: 85–98.

Huang, J. and Turcotte, D.L., 1989. Fractal mapping of digitized images: Application to the topography of Arizona and comparison with synthetic images. J. Geophys. Res., 94: 7491–7495.

King, G.C.P., Stein, R.S. and Rundle, J.B., 1988. The growth of geologic structures by repeated earthquakes, 1, Conceptual framework. J. Geophys. Res., 93: 13,307–13,318.

Kirkby, M.J., 1986. A two-dimensional simulation model for slope and stream evolution. In: A.D. Abrahams (Editor), Hillslope Processes. Binghampton Symp. Geomorph.,, Int. Ser. 16, George Allen and Unwin, Boston, pp. 203–222.

Koons, P.O., 1989. The topographic evolution of collisional mountain belts: A numerical look at the southern Alps, New Zealand. Am. J. Sci., 289: 1041–1069.

Lifton, N.A. and Chase, C.G., 1992. Tectonic, climatic and lithologic influences on landscape fractal dimension and hypsometry: implications for landscape evolution in the San Gabriel Mountains, California. In: R.S. Snow and L. Mayer (Editors), Fractals in Geomorphology. Geomorphology, 5: 77–113 (this issue).

Mandelbrot, B., 1982. The Fractal Geometry of Nature. Freeman, New York, N.Y., 460 pp.

Mandelbrot, B.B., 1989. Multifractal measures, especially for the geophysicist. Pure Appl. Geophys., 131: 5–42.

Mark, D.M. and Aronson, P.B., 1984. Scale-dependent fractal dimensions of topographic surfaces: An empirical investigation with applications in geomorphology and computer mapping. Math. Geol, 16: 671–683.

Mayer, L. and Chase, C.G., 1989. Use of fractal dimension in studies of the evolution of tectonic mountain fronts – measurement and interpretations. Geol. Soc. Am. Abstr. with Programs, 21: A38.

Molnar, P. and Lyon-Caen, H., 1988. Some simple physical aspects of the support, structure and evolution of mountain belts. In: S.P. Clark Jr., B.C. Burchfiel and J. Suppe (Editors), Processes in Continental Lithospheric Deformation. Geol. Soc. Am., Spec. Pap., 218: 179–207.

Roy, A.G., Gravel, G. and Gauthier, C., 1987. Measuring the dimension of surfaces: a review and appraisal of different methods. In: N.R. Chrisman (Editor), Auto Carto 8. Eight International Symposium on Computer-Assisted Cartography, pp. 68–77.

Sprunt, B., 1972. Digital simulation of drainage basin development. In: R.J. Chorley (Editor), Spatial Analysis in Geomorphology. Methuen, London, pp. 371–389.

Stein, R.S., King, G.C.P. and Rundle, J.B., 1988. The growth of geologic structures by repeated earthquakes, 2, Field examples of continental dip-slip faults. J. Geophys. Res., 93: 13,319–13,331.

Turcotte, D.L., 1991. Fractals in geology: What are they and what are they good for? GSA Today, 1: 1–4.

Von Neumann, J., 1966. Theory of automata: construction, reproduction, homogeneity. In: A.W. Burks (Editor), Theory of Self-Reproducing Automata. University of Illinois Press, Urbana, Ill., pp. 91–378.

Voss, R.F., 1988. Fractals in nature: From characterization to simulation. In: H.-O. Peitgen and D. Saupe (Editors), The Science of Fractal Images. Springer-Verlag, New York, N.Y., pp. 21–70.

Wolman, M.G. and Gerson, R., 1978. Relative scales of time and effectiveness of climate in watershed geomorphology. Earth Surf. Processes Landforms, 3: 189–208.

Wolman, M.G. and Miller, J.P., 1960. Magnitude and frequency of forces in geomorphic processes. J. Geol., 68: 54–74.

Woodward, J.A., 1990. The role of lithology and non-tectonic base-level change on the development of three pediment levels, southwestern Santa Catalina Mountains, Arizona M.S. Thesis, University of Arizona, Tucson, Ariz., 44 pp.